Available online at www.sciencedirect.com

SciVerse ScienceDirect

Ceramics International 39 (2013) 8267–8271

CERAMICS INTERNATIONAL

www.elsevier.com/locate/ceramint

# Thermal expansion behavior of La-doped $(Ba_{0.5}Sr_{0.5}Co_{0.8}Fe_{0.2})O_{3-\delta}$ cathode material

Bo-Kyung Kang[a], Ho-Chang Lee[a], Young-Woo Heo[a], Jeong-Joo Kim[a], Jae Yuk Kim[b], Joon-Hyung Lee[a,*]

[a]School of Materials Science and Engineering, Kyungpook National University, Daegu 702-701, Republic of Korea
[b]Ssangyong Materials Corp., Daegu 704-832, Republic of Korea

Received 8 March 2013; received in revised form 2 April 2013; accepted 3 April 2013
Available online 12 April 2013

**Abstract**

In this study, the thermal expansion behavior of the BSCF ($Ba_{0.5}Sr_{0.5}Co_{0.8}Fe_{0.2}O_{3-\delta}$) and La-doped BSCF, i.e., $(Ba_{0.5}Sr_{0.5})_{0.7}La_{0.3}Co_{0.8}Fe_{0.2}O_{3-\delta}$ (BSLCF30) was systematically examined. The thermal expansion rate of the sintered body increased rapidly at around 500 °C. It was found from the TG analysis that the oxygen vacancies formed around this temperature. When La is doped in the A-site of BSCF, more weight loss was observed over 500 °C compared to BSCF, which shows that La doping induces oxygen vacancies. Consequently, chemical expansion of the B-site cations occurred. Therefore, the thermal expansion coefficient (TEC) of BSLCF was much bigger than that of the BSCF. When the samples were heated and cooled in an Ar atmosphere, hysteresis of TEC was observed since re-oxidation cannot occur during cooling.


*Keywords:* C. Thermal expansion; Cathode; Solid oxide fuel cell; Chemical expansion; Oxygen vacancy

## 1. Introduction

Fuel cells are devices that converts the chemical reaction between hydrogen and oxygen to electric energy. They have received attention as an eco-friendly energy resource, because they have a high thermal efficiency without discharging pollutants. Among fuel cells, the solid oxide fuel cell has the highest efficiency in energy conversion. However, it also has many problems including thermal resistance, chemical stability, long-term reliability, etc, due to its high operation temperatures (700–1000 °C) [1–3].

In recent years, great efforts have been devoted to reduce the operation temperatures of solid oxide fuel cells (SOFCs). A lower operating temperature can suppress the degradation of components and extend the range of acceptable material selection. However, because a low operation temperature decreases the electrode kinetics, it leads to large interfacial polarization resistances. There fore, the cathode materials should be characterized by increased oxide ion transport in addition to high electronic conductivity [4,5].

Recently, various perovskite oxides have been used as cathode materials for intermediate temperature SOFC (IT-SOFC), including $La_{0.6}Sr_{0.4}Co_{0.2}Fe_{0.8}O_{3-\delta}$ (LSCF) and $Ba_{0.5}Sr_{0.5}Co_{0.2}Fe_{0.8}O_{3-\delta}$ (BSCF) [6–8]. BSCF is particularly attracting attention as a potential cathode material for IT-SOFCs, due to its high ionic conductivity and high energization. However, BSCF has the disadvantage of low electric conductivity. Many different compositions with lanthanides and Sr or Ca on the A-site and with Mn, Fe, Co and Ni on the B-site have been proposed as alternative cathode materials.

Recent studies have tried to substitute rare earth metal ions for the A-site of BSCF. As a result, their properties were greater than those of the undoped BSCF, and they had greater values not only in electrical properties but also in electrochemical properties [9–11]. Apart from high electrical and electrochemical properties, the new cathode materials must have matched thermal expansion coefficients, because a cell consists of several layers of different materials in constant contact with each other, which is one of the most important criteria for mechanical stability of such a multi-component system [12,13].

In this study, the effects of La doping on the thermal expansion behaviors of BSCFs were systematically analyzed. High temperature X-ray diffraction, thermogravimetry (TG) and

*Corresponding author. Tel.: +82 53 9507512; fax: +82 53 9505645.
*E-mail address:* joonlee@knu.ac.kr (J.-H. Lee).

0272-8842/$ - see front matter © 2013 Elsevier Ltd and Techna Group S.r.l. All rights reserved.
http://dx.doi.org/10.1016/j.ceramint.2013.04.012

X-ray photoelectron spectroscopy (XPS) analysis were also conducted.

## 2. Experimental procedure

The $Ba_{0.5}Sr_{0.5}Co_{0.8}Fe_{0.2}O_{3-\delta}$ (here after BSCF) and $(Ba_{0.5}Sr_{0.5})_{0.7}La_{0.3}Co_{0.8}Fe_{0.2}O_{3-\delta}$ (here afterwards BSLCF) powders were prepared by conventional solid-state reaction methods using $BaCO_3$, $SrCO_3$, $La_2O_3$, $Co_3O_4$ and $Fe_2O_3$ as raw materials. These powders were mixed under ethanol and milled for 24 h using zirconia balls. The ball-milled mixture was dried and ground, and then calcined in air at 1150 °C for 2 h. The calcined powders were ball-milled for a second time to break any agglomerations during the calcination process.

The synthesized powders were pressed into pellets, and then were cold-isostatically pressed at 100 MPa. The samples were sintered at 1200 °C for 2 h at a heating rate of 5 °C/min and coo led at the natural cooling rate of the furnace in air. The density of the pellets was about 94–97% of the theoretical value as determined by Archimedes' method.

Crystal structures of the synthesized powders were characterized by a high temperature X-ray diffractometer (XRD; D/MAX-2500, Rigaku) with Cu-Kα radiation at both room temperature and high temperatures. Thermogravimetry analysis (TGA; SCINCO STA S-1500) was performed from 50 °C to 800 °C, and dilatometric measurements were performed using a TMA (Bruker TD5000SA) in the temperature range of 30–800 °C in air, oxygen and argon with a heating rate of 2 °C/min. The chemical bonding states of the BSCF and BSLCF at room temperature and 700°C were analyzed by means of X-ray photoelectron spectroscopy (XPS; Thermo Fisher Scientific, Theta Probe AR-XPS) spectrometer. XPS was carried out using a monochromated Al-Kα (1486.6 eV) X-ray source. The initial vacuum pressure of the XPS chamber was in the order of $10^{-9}$ Torr. However, when the sample is heated for the analysis at 700°C, because of outgassing from the samples, ramp up was stopped and evacuation process was continued until the vacuum drops to $10^{-7}$ Torr.

## 3. Results and discussion

Fig. 1 shows the X-ray diffraction patterns of the BSCF and BSLCF powders synthesized by the general solid-state reaction process. The result shows that both of the BSCF and BSLCF have a cubic perovskite structure. In addition, the main peaks of BSLCF were shifted to a higher angle than those of BSCF. This result shows that the lattice constant of the perovskite was decreased by the substitution of $La^{3+}$ ions for the $Ba^{2+}$ and $Sr^{2+}$ ions. This was because the ionic radius of $La^{3+}$(1.36 Å) is smaller than that of $Ba^{2+}$(1.61 Å) and $Sr^{2+}$(1.44 Å). Lattice constants, calculated from the XRD patterns, were 4.00 Å and 3.89 Å, for the BSCF and BSLCF, respectively.

Fig. 2 shows the lattice constants of the BSCF and BSLCF samples as a function of the temperature evaluated from the high temperature X-ray diffraction patterns. The lattice constants slowly increased up to 500 °C, however, they greatly increased when the temperature rose over 500 °C. Concerning

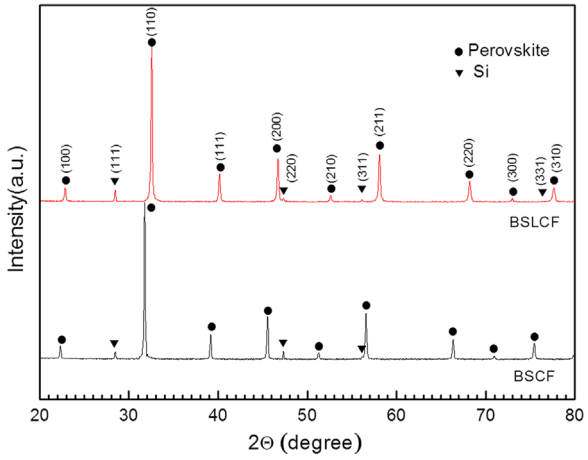


Fig. 1. X-ray diffraction patterns of the BSCF and BSLCF powders calcined at 1150 °C for 2 h in air.

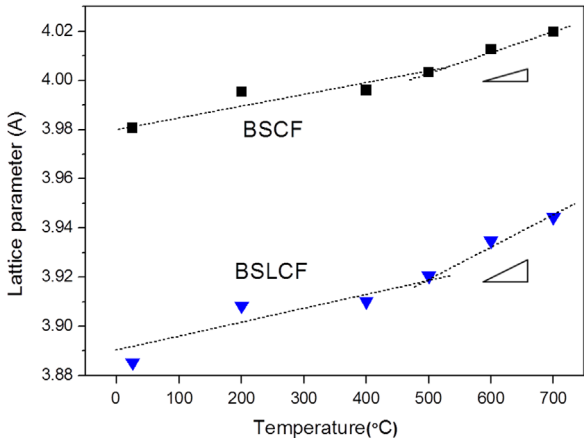


Fig. 2. Lattice parameters of the BSCF and BSLCF samples measured by a high temperature X-ray diffraction at different temperatures.

the slope of the lattice constant over 500 °C, the BSLCF revealed a higher slope than that of the BSCF.

Fig. 3 shows the thermogravimetric weight loss and thermal expansion measurements for the samples, which were sintered at 1200 °C for 2 h. The measurements were conducted in air. As the temperature increased, there was no significant change in weight loss up to about 500 °C. However, weight loss rapidly increased after the temperature reached 500 °C. Note that the weight loss of BSLCF begins at around 495 °C while that of BSCF begins at a higher temperature around 550 °C. Concerning the thermal expansion, it increased slowly and linearly up to 500 °C, and then, it increased sharply after 500 °C. This result coincides with the lattice constant shown in Fig. 2. In the case of the BSLCF, TEC increased almost twice as much as that of the BSCF at high temperature around 800 °C.

Concerning the weight loss at low temperature up to 250 °C, it was considered to have occurred due to the evaporation of the physisorbed water molecules and desorption of carbon dioxide. The rapid weight loss which occurred at 500 °C can mainly be attributed to the release of lattice oxygen [14,15]. Total weight loss was 0.43% for BSCF, and 0.86% for BSLCF at 800 °C,

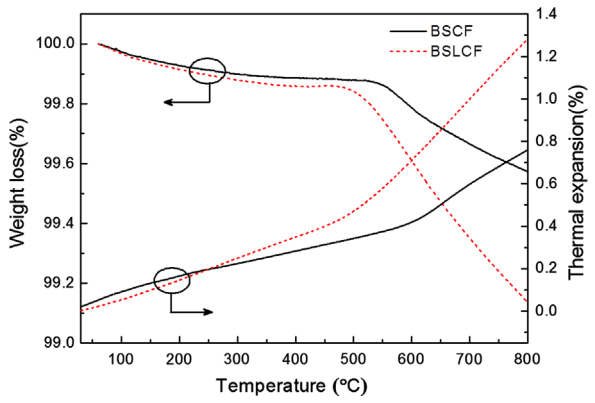


Fig. 3. Thermal expansion behaviors and thermalgravimetry curves of the BSCF and BSLCF sintered rods analyzed in air.

i.e., the weight loss of BSLCF was twice that of the BSCF. As the temperature rises, the amount of oxygen vacancies increases. In this case, if bridging oxygen ions are removed, the cation–cation repulsion would increase. Then, the lattice expansion might also increase [16].

Simultaneously, the reduction of the Fe and Co ions from a high to a lower valence state must occur in order to maintain the electrical neutrality [17–19], which will result in a large chemical expansion.

In order to identify the valence states of the cations, XPS analyses at room temperature and at 700 °C were conducted. Coincidently, the peak position of $Co2p_{3/2}$ is very close to that of $Ba3d_{5/2}$ and a neat deconvolution of the peaks is difficult. Both the BSCF and BSLCF did not show any significant differences, the XPS results of the BSLCF at room temperature and 700 °C are shown in Fig. 4(a). The locations of the peaks at room temperature are marked by numbered arrows. The two peaks merged into one and the width of the peak decreased and the intensity increased when the temperature increased. This seems to be caused by the intensity change, i.e., valence change from $Co^{4+}$ and/or $Co^{3+}$ to $Co^{2+}$ as the lattice oxygen is released at high temperature. However, a chemical shift of about 0.6 eV to a higher binding energy was observed in Ba4d located around 80–95 eV at 700 °C. This also might be contributed to a change in the peak shape. Concerning the Fe ions in Fig. 4(b), it is difficult to distinguish between $Fe^{3+}$ and $Fe^{4+}$ because $Fe^{3+}$ coexists with $Fe^{4+}$ at RT with oxygen deficiency in$BaFeO_{3-\delta}$ [20] and the bonding strength of $Fe^{3+}$–$O^{2-}$ and $Fe^{4+}$–$O^{2-}$ are almost identical [21]. However, the XPS spectra of $Fe^{3+}$ (711 eV) and $Fe^{2+}$ (709 eV) ions are distinguishable [22] and increase in intensity around the $Fe^{2+}$ position shown in Fig. 4(b) at 700 °C. The $O_{1s}$ spectra for the BSLCF are shown in Fig. 4 (c). The $O_{1s}$ spectra at RT present a broad peak, at 700 °C, however, the overall peak area decreased and the noticeable peak intensity at around 529–532 eV decreased. The BE peak at around 528 eV is ascribed to the lattice oxygen species, $O^{2-}$ [23,24]. The other peak (529.2 eV) is assigned to less adsorbed oxygen species, $O_2^{2-}/O^-$, referred to as electrophilic oxygen [23–25] and the BE peak (531.0 eV) corresponds to $CO_3^{2-}$ or $OH^-$ [23–26].

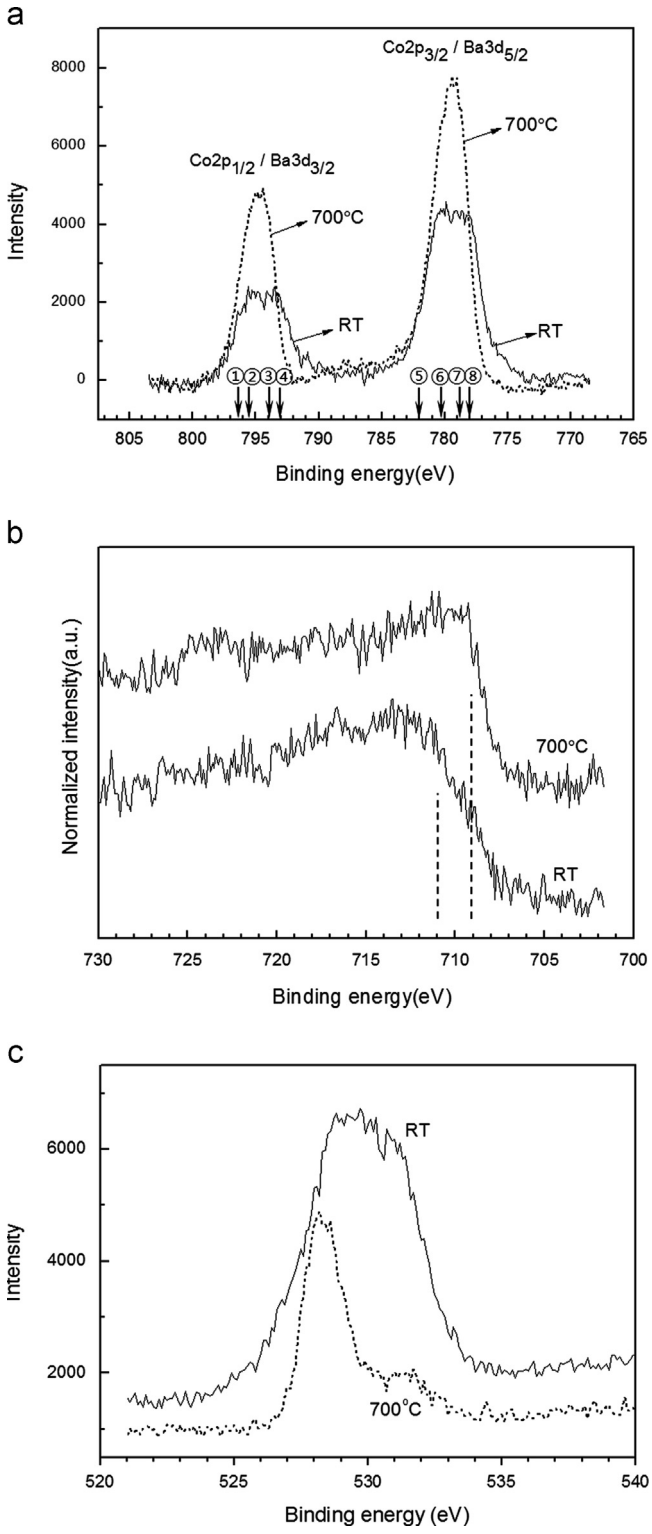


Fig. 4. Chemical shift of (a) $Ba3d_{3/2}$ and $Co2p_{1/2}$, (b) $Fe2p_{3/2}$ and (c) $O_{1s}$ for the BSLCF sintered sample at room temperature and 700 °C. In (a), ① and ⑤ correspond to $Co^{4+}$, ② and ⑥: $Co^{3+}$, ③ and ⑦: $Co^{2+}$, ④ and ⑧: $Ba^{2+}$.

Thermal expansion coefficient (TEC) of the BSCF and BSLCF samples were analyzed in Ar, air and $O_2$ atmospheres, from room temperature to 800 °C. Table 1 shows the average TEC of the samples, measured under different oxygen partial

pressures, from 600 °C to 800 °C where the oxygen release is active. Average TEC at high temperature for both BSCF and BSLCF increased, as the oxygen partial pressure decreased. In the case of the BSLCF, despite the smaller lattice constant shown in Figs. 1 and 2, its TEC value was much larger than that of the BSCF in all atmospheres. This result shows that La doping contributed to the increase in TEC due to the increase in the formation of oxygen vacancies.

Fig. 5 shows the thermal expansion behavior of the sintered body during heating and cooling, in (a) Ar and (b) oxygen atmospheres. During heating in Ar, a linear thermal expansion behavior was shown up to 450 °C (BSLCF) or 550 °C (BSCF). In this case, the slopes of the expansion for the BSCF and BSLCF are almost the same. However, over 500–550 °C where the oxygen vacancies are produced energetically, the thermal expansion slope increased due to the additional expansion factors for the formation of oxygen vacancies as well as chemical expansion. Particularly, a great increase in the slope of the BSLCF over 500 °C is notable, because, BSLCF creates more oxygen vacancies than that of BSCF at high temperatures shown in Fig. 3. After cooling in an Ar atmosphere, a bigger hysteresis of thermal expansion was observed in the BSLCF. This was because re-oxidation cannot occur during cooling in the Ar atmosphere. Interestingly, a rough estimation of the slopes in the BSLCF during cooling and heating from 800 °C to RT and from RT to 450 °C is almost the same. This signifies that the shrinkage in-argon is only dependent on temperature and no chemical shrin kage is involved. The lattice constant of the BSLCF rod sample before heating and after cooling increased from 3.89 Å to 3.98 Å.

However, when the samples were heated and cooled in an oxygen atmosphere in Fig. 5(b), a weak chemical expansion from the oxygen release also appeared. However, it fully recovered during the cooling process by oxidation. Furthermore, because the samples were sintered in air, a certain amount of nonstoichiometric oxygen ($\delta$ value in $(Ba_{0.5}Sr_{0.5})_{0.7}La_{0.3}Co_{0.8}Fe_{0.2}O_{3-\delta}$) exists and the cooling in oxygen resulted in a decrease in the $\delta$ which resulted in expansion-induced hysteresis. From the results of Fig. 5, it is revealed that the oxygen nonstoichiometry ($\delta$) of BSLCF is more dependent on the oxygen partial pressure than that of the BSCF.

When the heating–cooling thermal cycle of the BSLCF sample was conducted 3 times in an Ar atmosphere, the heating and cooling curves of the second and third cycling of the sample al-most overlapped the cooling curve of the first cycle (see Fig. 6). Therefore, thermal expansion and shrinkage curves for the second and third cycling remained unchanged. After measuring the thermal expansion behavior in the Ar atmosphere, the lattice constant of the sample increased from 3.89 Å to 3.93 Å, due to cation–cation repulsion and chemical expansion.

Table 1
Average TEC values of the BSCF and BSLCF samples in temperatures ranging from 600–800 °C analyzed under argon, air and oxygen atmospheres.

| Sample | TEC ($10^{-6}$ $K^{-1}$) at 600–800 °C | | |
|---|---|---|---|
| | Ar | Air | $O_2$ |
| BSCF | 21.22 | 18.96 | 18.21 |
| BSLCF | 33.71 | 28.38 | 25.30 |

## 4. Conclusion

In this study, the thermal expansion behavior of BSCF and La-doped BSCF (BSLCF), which is one of the potential cathode materials for IT-SOFC, was investigated. Thermal expansion of the sintered samples increased slowly and linearly as the temperature increased up to 500 °C. However, it rapidly increased over 500 °C. From the TG analysis and repetitive heating–cooling cycle experiments of the samples in Ar gas, it was found that the formation of oxygen vacancies made the thermal and chemical expansion increase sharply. Especially La doping promoted the formation of oxygen vacancies in BSCF at high temperatures in which SOFCs generally operate.

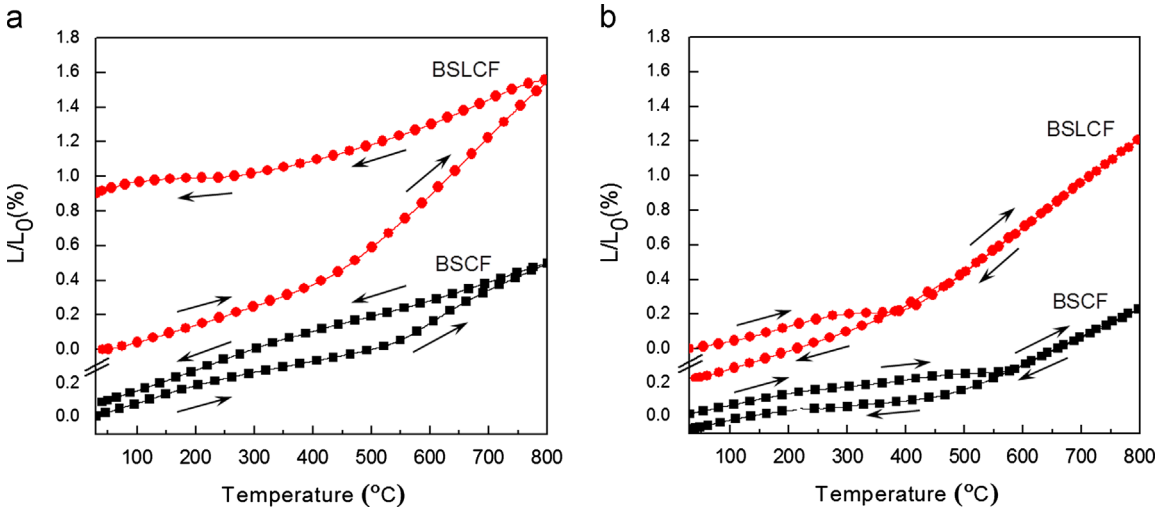


Fig. 5. Thermal expansion behaviors of the BSCF and BSLCF sintered rods analyzed in (a) argon and (b) oxygen atmospheres.

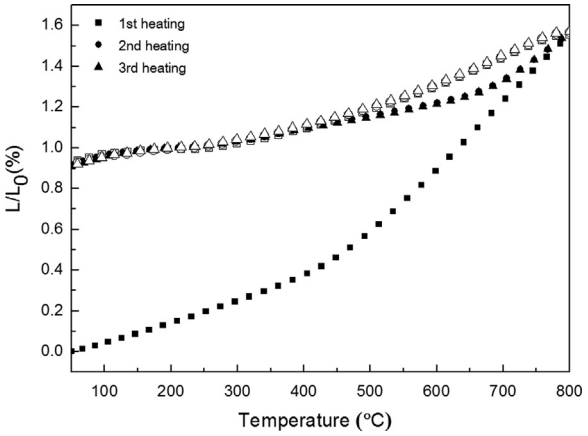


Fig. 6. Repetitive thermal expansion behavior of a BSLCF rod analyzed in an argon atmosphere.

Although $La^{3+}$ doping in the A-site plays the role of the donor, when taking the TG, XPS and TEC results all together, the donor has not been well compensated by the B-site ions of Co and Fe in the BSCF, and it provoked the formation of oxygen vacancies. The increased oxygen vacancies increased the TEC, and the TEC value of BSLCF was twice as high as that of the GDC ($12.6 \times 10^{-6}$/K). Consequently, even though some rare earth metal ions are doped for the A-site of BSCF for an improved electrical and electrochemical properties, the rapid increase of TEC at high temperature is an obvious negative effect to avoid.

## Acknowledgments

This research was financially supported by the Ministry of Education, Science Technology (MEST) and National Research Foundation of Korea (NRF) through the Human Resource Training Project for Regional Innovation. This work was also supported by the National Research Foundation of Korea Grant (2011-0020264, 2011-0012678, 2011-0017245) funded by the South Korean Government. XPS (Theta Probe XPS system) analysis of the samples was kindly provided by Dr. Jong-Seong Bae at Korea Basic Science Institute Busan Center, Korea. This research was supported by Kyungpook National University Research Fund, 2012.

## References

[1] S.C. Singhal, K. Kendall, High Temperature Solid Oxide Fuel Cells: Fundamentals, Design, and Applications, Elsevier, Oxford1–22.
[2] V. Gil, J. Tartaj, C. Moure, Chemical and thermomechanical compatibility between Ni-GDC anode and electrolytes based on ceria, Ceramics International 35 (2009) 839–846.
[3] I.M. Hung, H.W. Peng, S.L. Zheng, C.P. Lin, J.S. Wu, Phase stability and conductivity of $Ba_{1-y}Sr_yCe_{1-x}Y_xO_{3-d}$ solid oxide fuel cell electrolyte, Journal of Power Sources 193 (2009) 155–159.
[4] C. Sun, R. Hui, J. Roller, Cathode materials for solid oxide fuel cells: a review, Journal of Solid State Electrochemistry 14 (2010) 1125–1144.
[5] A. Princivalle, E. Djurado, Nanostructured LSM/YSZ composite cathodes for IT-SOFC: a comprehensive microstructural study by electrostatic spray deposition, Solid State Ionics 179 (2008) 1921–1928.
[6] Z. Shao, J. Mederos, W.C. Chueh, S.M. Haile, High power-density single-chamber fuel cells operated on methane, Journal of Power Sources 162 (2006) 589–596.
[7] H. Lu, J. Tong, Y. Cong, W. Yang, Partial oxidation of methane in $Ba_{0.5}Sr_{0.5}Co_{0.8}Fe_{0.2}O_{3-\delta}$ membrane reactor at high pressures, Catalysis Today 104 (2005) 154–159.
[8] J.F. Vente, W.G. Haije, Z.S. Rak, Performance of functional perovskite membranes for oxygen production, Journal of Membrane Science 276 (2006) 178–184.
[9] S.Y. Li, Z. Lu, N. Ai, K.F. Chen, W.H. Su, Electrochemical performance of $(Ba_{0.5}Sr_{0.5})_{0.9}Sm_{0.1}Co_{0.8}Fe_{0.2}O_{3-\delta}$ as an intermediate temperature solid oxide fuel cell cathode, Journal of Power Sources 165 (2007) 97–101.
[10] O.A. Marina, N.L. Canfield, J.W. Stevenson, Thermal, electrical, and electrocatalytical properties of lanthanum-doped strontium titanate, Solid State Ionics 149 (2002) 21–28.
[11] S. Li, Z. Lu, X. Huang, B. Wei, W. Su, Thermal, electrical, and electrochemical properties of Lanthanum-doped $Ba_{0.5}Sr_{0.5}Co_{0.8}Fe_{0.2}O_{3-\delta}$, Journal of Physics and Chemistry of Solids 68 (2007) 1707–1712.
[12] B.C.H. Steele, Oxygen-transport and exchange in oxide ceramics, Journal of Power Sources 49 (1994) 1–14.
[13] A. Bieberle, L.J. Gauckler, Thermal and isothermal expansion, in: H.L. Tuller, J. Schoonman, I. Riess (Eds.), Oxygen Ion and Mixed Conductors and their Technological Applications, Kluwer Academic Publishers, Dordrecht, The Netherlands, 2000, pp. 347–358.
[14] S. McIntosh, J.F. Vente, W.G. Haije, D.H.A. Blank, H.J. M. Bouwmeester, Oxygen stoichiometry and chemical expansion of $Ba_{0.5}Sr_{0.5}Co_{0.8}Fe_{0.2}O_{3-\delta}$ measured by in situ neutron diffraction, Chemistry of Materials 18 (2006) 2187–2193.
[15] R. Kriegel, R. Kircheisen, J. Töpfer, Oxygen stoichiometry and expansion behavior of $Ba_{0.5}Sr_{0.5}Co_{0.8}Fe_{0.2}O_{3-\delta}$, Solid State Ionics 181 (2010) 64–70.
[16] S.M. Kim, K.H. Seo, J.H. Lee, J.J. Kim, H.Y. Lee, J.S. Lee, Preparation and sintering of nanocrystalline ITO powders with different $SnO_2$ content, Journal of the European Ceramic Society 26 (2006) 73–80.
[17] L.-W. Tai, M.M. Nasrallash, H.U. Anderson, D.M. Sparlin, S.R. Sehlin, Structure and electrical properties of $La_{1-x}Sr_xCo_{1-y}Fe_yO_3$. Part 1: the system $La_{0.8}Sr_{0.2}Co_{1-y}Fe_yO_3$, Solid State Ionics 76 (1995) 259–271.
[18] G.Ch. Kostogloudis, P. Fertis, Ch. Ftikos, The perovskite oxide system $Pr_{1-x}Sr_xCo_{1-y}Mn_yO_{3-\delta}$: crystal structure and thermal expansion, Journal of the European Ceramic Society 18 (1998) 2209–2215.
[19] A.L. Shaula, V.V. Kharton, N.P. Vyshatko, E.V. Tsipis, M.V. Patrakeev, F.M.B. Marques, J.R. Frade, Oxygen ionic transport in $SrFe_{1-y}Al_yO_{3-\delta}$ and $Sr_{1-x}Ca_xFe_{0.5}Al_{0.5}O_{3-\delta}$ ceramics, Journal of the European Ceramic Society 25 (2005) 489–499.
[20] K. Mori, T. Kamiyama, H. Kobayashi, K. Itoh, T. Otomo, S. Ikeda, Local structure of $BaFeO_{3-\delta}$ studied by neutron scattering, Physica B 329–333 (2003) 807–808.
[21] H. Falcon, J.A. Barbero, J.A. Alonso, M.J. Martınez-Lope, J.L.G. Fierro, $SrFeO_{3-\delta}$ perovskite oxides: chemical features and performance for methane combustion, Chemistry of Materials 14 (2002) 2325–2333.
[22] T. Yamashita, P. Hayes, Analysis of XPS spectra of $Fe^{2+}$ and $Fe^{3+}$ ions in oxide materials, Applied Surface Science 254 (2008) 2441–2449.
[23] J.I. Jung, D.D. Edwards, X-ray photoelectron (XPS) and Diffuse Reflectance Infra Fourier Transformation (DRIFT) study of $Ba_{0.5}Sr_{0.5}$-$Co_xFe_{1-x}O_{3-\delta}$ (BSCF: $x$=0–0.8) ceramics, Journal of Solid State Chemistry 184 (2011) 2238–2243.
[24] J.I. Jung, D.D. Edwards, X-ray photoelectron study on $Ba_{0.5}Sr_{0.5}Co_xFe_{1-x}O_{3-\delta}$ (BSCF: $x$=0.2 and 0.8) ceramics annealed at different temperature and $pO_2$, Journal of Materials Science 46 (2011) 7415–7422.
[25] N.A. Merino, B.P. Barbero, P. Eloy, L.E. Cadus, Applied Surface Science 253 (2006) 1489.
[26] S. Rousseau, S. Loridant, P. Delichere, A. Boreave, J.P. Deloume, P. Vernoux, Applied Catalysis B 88 (2009) 438.